



Trapped and Unstable: Axion-like particle fragmentation at finite temperature

Nicklas Ramberg ^{1,2,3,*} and Daniel Schmitt ^{4,†}

¹*SISSA International School for Advanced Studies, Via Bonomea 265, 34136, Trieste Italy*

²*INFN Sezione di Trieste, Via Bonomea 265, 34136, Trieste Italy*

³*IFPU, Institute for Fundamental Physics of the Universe, Via Beirut 2, 34014 Trieste, Italy*

⁴*Institute for Theoretical Physics, Goethe University, 60438 Frankfurt am Main, Germany*

(Dated: November 14, 2025)

We investigate the emergence of a resonant behavior in axion-trapped misalignment models featuring finite-temperature potential barriers. As the temperature decreases and the field is released from its trapped configuration, inhomogeneities are exponentially amplified through an instability in their equation of motion, leading to the fragmentation of the axion field. We show that this process constitutes a novel source of gravitational waves (GWs), analogous to those generated in zero-temperature axion fragmentation, but with distinct characteristics. We quantify the resulting GW spectrum, identifying the peak frequency and amplitude associated with the inhomogeneous axion dynamics. Our results indicate that the GW signal can be enhanced by up to two orders of magnitude compared to the standard fragmentation scenario, while exhibiting a markedly different spectral shape. The parameter space featuring both strong GW signals and reproducing the correct dark matter abundance is, however, limited.

INTRODUCTION

The QCD axion was originally introduced to resolve the strong CP problem in quantum chromodynamics (QCD) through the Peccei–Quinn (PQ) mechanism [1–3]. Beyond this motivation, the axion also stands out as a compelling candidate for cold dark matter (CDM), produced non-thermally through the misalignment mechanism [4–6]. In so-called trapped misalignment models, the axion potential acquires additional contributions in the form of explicit PQ-breaking or temperature-dependent operators, generating additional minima separated by a barrier [7–10]. For exceptionally light axions in the pre-inflationary scenario, ultraviolet (UV) completions based on discrete \mathbb{Z}_N symmetries have been proposed as a natural realization of this framework [11]. Meanwhile, for post-inflationary PQ breaking, the QCD axion model is particularly predictive, leaving only a narrow window of viable parameter space [12–15].

More generally, pseudoscalar fields arising as pseudo–Nambu–Goldstone bosons of broken global symmetries are referred to as axion-like particles (ALPs). Such fields appear abundantly in string theory compactifications [16–19] and have also been considered as potential inflaton candidates [20–26]. In this work, we focus on pre-inflationary ALPs as the underlying field content, while noting that the mechanism we propose may also find realization within QCD axion models.

In particular, we study ALPs that are initially trapped by a thermal barrier [10, 27]. Then, the ALP remains in a metastable minimum until the barrier disappears, after which it rolls towards the true vacuum. We show that the delayed onset of oscillations triggers a resonance in the ALP equation of motion, leading to a copious production of ALP quanta in the early Universe, resulting in

the fragmentation of the ALP field [28–34].¹ Intriguingly, the generation of long-wavelength fluctuations generates anisotropies in the energy-momentum tensor of the cosmic fluid that act as a source of stochastic GWs [36–47].

A stochastic gravitational wave background (SGWB) generated in the pre-nucleosynthesis universe propagates almost entirely undisturbed until today, hence offering deep insights into the physics of the very early universe, if ever observed [48]. While typical sources include, for example, first-order phase transitions [49–59], ALPs are attracting growing interest as a source of GWs [27, 60–73]. In particular, GW emission from axion fragmentation has been explored in monodromy [29] and kinetic misalignment [31] scenarios. In this work, we show that trapped misalignment provides initial conditions that lead to ALP fragmentation and estimate the GW signal both analytically and numerically. Remarkably, initial trapping significantly enhances the GW amplitude compared to previous works. We further compute the ALP relic abundance, finding that simultaneously generating large GW amplitudes and the correct CDM abundance is hard to realize.

We structure this paper as follows. First, we outline the model and calculate the analytic conditions for the release temperature and angle. Then, we identify the instability band, derive the conditions for efficient growth, and perform a numerical analysis of the resonant behavior. We compute the GW spectrum for different benchmarks and discuss its characteristics, demonstrating that trapped misalignment offers a viable GW source.

¹ Note that such dynamics are absent in the standard misalignment mechanism, unless the initial misalignment angle is tuned close to the potential maximum [35].

THERMALLY TRAPPED MISALIGNMENT

In the ordinary misalignment mechanism, one considers an ALP ϕ with a potential

$$V(\phi) = m_\phi^2 f_\phi^2 \left(1 - \cos\left(\frac{\phi}{f}\right) \right). \quad (1)$$

Initially displaced by the misalignment angle $\theta_i \sim \mathcal{O}(1)$, the ALP starts to oscillate around the potential minimum as the Hubble parameter drops below the ALP mass $H \sim m_\phi$. This corresponds to the temperature

$$T_{\text{osc}}^{\text{mis}} = \left(\frac{90}{\pi^2 g_\epsilon} \right)^{\frac{1}{4}} \sqrt{m_\phi M_{\text{Pl}}}. \quad (2)$$

Here, g_ϵ denotes the effective relativistic degrees of freedom and M_{Pl} is the reduced Planck mass. Subsequently, the ALP energy density follows a matter-like scaling $\rho_\phi \propto a^{-3}$, making the pseudoscalar a viable CDM candidate.

Trapped misalignment has been suggested as an alternative mechanism for ALP production in the early Universe [8–10]. Here, further explicit PQ-breaking terms alter the structure of the ALP potential, generating additional minima. This can trap the ALP in a false minimum, thereby delaying the onset of ALP oscillations. In this work, we consider the temperature-dependent trapping potential from [10, 27]

$$V(\phi, T) = m_\phi^2 f_\phi^2 \left(1 - \cos\left(\frac{\phi}{f_\phi}\right) \right) + \Lambda_{\cancel{\text{PQ}}}^{4-q} T^q \left(1 - \cos\left(n \frac{\phi}{f_\phi} + \delta\right) \right), \quad (3)$$

where m_ϕ is the axion mass, f_ϕ its decay constant, $\Lambda_{\cancel{\text{PQ}}}$ is the energy scale at which explicit PQ breaking operators emerge, n denotes the multiplicity of minima, and δ is the phase shift. For simplicity, we focus on $n = 2$ hereafter.² An exemplary ALP potential is shown in fig. 1. At high temperature, the T -dependent terms in the potential (3) generate a false minimum that vanishes at the release temperature $T = T_{\text{rel}}$. The time when the field is released from the trapping potential is defined by the following conditions:

$$\frac{\partial V(\phi, T)}{\partial \phi} = 0, \quad \frac{\partial^2 V(\phi, T)}{\partial \phi^2} = 0. \quad (4)$$

This corresponds to a saddle point in the potential. In the following, we analytically derive approximate conditions on the model parameters for trapping to terminate.

First, from eq. (4) we find a relation for the position of the false minimum, i.e., the release angle

$$\tan(\theta_{\text{rel}}) = \frac{1}{n} \tan(n\theta_{\text{rel}} + \delta). \quad (5)$$

In the case of $n = 2$ one can reformulate the equation into an algebraic trigonometric equation of cubic order

$$2 \tan^3(\theta_{\text{rel}}) + 3 \tan(\delta) \tan^2(\theta_{\text{rel}}) + \tan(\delta) = 0. \quad (6)$$

If $\delta = 0$, the equation becomes a triple-root. For small but non-zero δ one can Taylor-expand $\tan(\delta) \approx \delta + \mathcal{O}(\delta^3)$, which reduces eq. (6) to

$$2t^3 + 3\delta t^2 + \delta = 0, \quad (7)$$

with $t = \tan(\theta_{\text{rel}})$. We will only concern ourselves with real-valued solutions to this equation, which can be shown to have the form

$$\theta_{\text{rel}} \simeq \arctan\left(-2^{-\frac{1}{3}}\delta^{\frac{1}{3}} - \frac{\delta}{2} + \mathcal{O}(\delta^{\frac{5}{3}})\right) + k\pi, \quad k \in \mathbb{Z}, \quad (8)$$

where k is an integer number. This can be finally formulated as

$$\theta_{\text{rel}} \simeq -2^{-\frac{1}{3}}\delta^{\frac{1}{3}} - \frac{\delta}{2} + \mathcal{O}(\delta^{\frac{5}{3}}) + k\pi, \quad k \in \mathbb{Z}. \quad (9)$$

In the above expression, $(\delta/2)^{1/3}$ is the leading-order term, and the linear term is second-order. We have checked its validity at T_{rel} and found that only using the first term in the expansion is sufficient to estimate the release temperature as a function of the initial angle. In full generality, one can solve eq. (6) for a certain value of δ and insert that value for θ_{rel} to then find T_{rel} .

We compute the release temperature by requiring that the ALP becomes massless at θ_{rel} defined by eq. (9). That is, we solve the second trapping condition (cf. eq. (4)), which gives

$$T_{\text{rel}} \approx \left(\frac{m_\phi^2 f_\phi^2 \cos(\theta_{\text{rel}})}{4\Lambda_{\cancel{\text{PQ}}}^{4-q} \cos(2\theta_{\text{rel}} + \delta)} \right)^{\frac{1}{q}}. \quad (10)$$

Finally, we need to check whether trapping actually takes place. If, e.g., $\Lambda_{\cancel{\text{PQ}}}$ is too small, we have $T_{\text{rel}} > T_{\text{osc}}^{\text{mis}}$, where the latter marks the onset of oscillations in the ordinary misalignment mechanism defined via $H = m_\phi$; see eq. (2). Then, $H_{\text{rel}} > m_\phi$, and the ALP would remain overdamped until the temperature drops to $T_{\text{osc}}^{\text{mis}}$. Therefore, we define the oscillation temperature as

$$T_{\text{osc}} = \min\{T_{\text{rel}}, T_{\text{osc}}^{\text{mis}}\}, \quad (11)$$

which is related to the Hubble parameter at the start of oscillations through

$$H_{\text{osc}} = \left(\frac{\rho_r}{3M_{\text{Pl}}^2} \right)^{\frac{1}{2}}, \quad (12)$$

with $\rho_r = (\pi^2/30)g_{\text{osc}}T_{\text{osc}}^4$ being the energy density of the radiation bath.

² Note that it is straightforward to extend our results to an arbitrary number of additional minima.

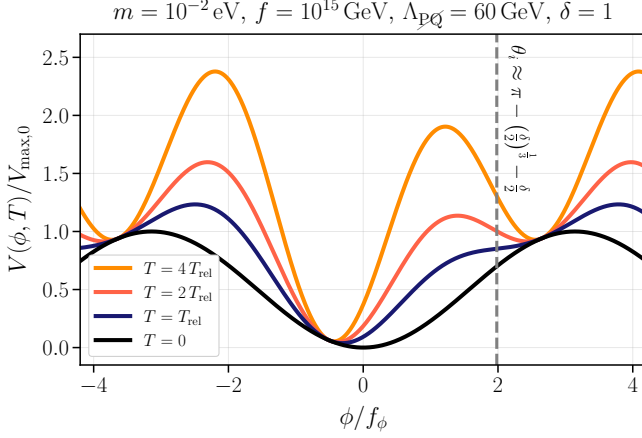


FIG. 1. Exemplary ALP potential (3), employing the indicated benchmark parameters. Initially, a thermal barrier prevents the ALP from rolling. As the barrier vanishes around T_{rel} , the false minimum becomes a saddle point and oscillations about the true minimum start. The numerical evaluation of the finite-temperature release angle (dashed gray) agrees well with our approximate solution (9).

ALP FRAGMENTATION

In this section, we outline the dynamics of the resonant behavior leading to the fragmentation of the ALP field, derive the conditions for efficient growth of fluctuations, and discuss the relic ALP abundance.

Equations of motion

The ALP equation of motion reads

$$\ddot{\phi} + 3H\dot{\phi} - \frac{1}{a^2}\nabla^2\phi + \frac{\partial V(\phi, T)}{\partial \phi} = 0, \quad (13)$$

where dots indicate derivatives with respect to cosmic time and a is the scale factor of the Universe. In this work, we restrict ourselves to a perturbative approach to compute the ALP evolution. That is, we decompose the pseudoscalar into a homogeneous mode and small fluctuations

$$\begin{aligned} \phi(t, \mathbf{x}) &= \phi(t) + \delta\phi(t, \mathbf{x}) \\ &= \phi(t) + \left(\int \frac{d^3k}{(2\pi)^3} a_k u_k(t) \exp(i\mathbf{k}\mathbf{x}) + \text{h.c.} \right). \end{aligned} \quad (14)$$

We introduce creation (a_k) and annihilation (a_k^\dagger) operators that satisfy the commutation relation $[a_k, a_{k'}^\dagger] = (2\pi)^3 \delta^{(3)}(k - k')$. The time evolution is governed by the mode functions $u_k(t)$, which we initialize in the Bunch-Davies vacuum. For small fluctuations $\delta\phi \ll \phi$, we can expand the derivative of

the potential as [28, 31]

$$\frac{\partial V}{\partial \phi} = \frac{\partial V}{\partial \phi} + \frac{\partial^2 V}{\partial \phi^2} \delta\phi + \frac{1}{2} \frac{\partial^3 V}{\partial \phi^3} \delta\phi^2 + \dots \quad (15)$$

Inserting this expression into eq. (13), switching to Fourier space, and employing conformal time τ , we obtain two coupled equations of motion:

$$\phi'' + 2aH\phi' + a^2 \frac{\partial V}{\partial \phi} + \frac{1}{2} \frac{\partial^3 V}{\partial \phi^3} \int \frac{d^3k}{(2\pi)^3} |u_k|^2 = 0, \quad (16)$$

$$u_k'' + 2aHu_k' + \left[k^2 + a^2 \frac{\partial^2 V}{\partial \phi^2} \right] u_k = 0. \quad (17)$$

Here, the last term in eq. (16) governs the backreaction from the fluctuations onto the zero mode.

In the limit of a negligible Hubble rate, eq. (17) reduces to a Mathieu equation [74], which exhibits a resonant behavior in certain momentum bands. The dominant instability band is approximately given by [28]

$$\frac{\dot{\phi}^2}{4f_\phi^2} - \frac{m_\phi^2}{2} \lesssim \left(\frac{k}{a} \right)^2 \lesssim \frac{\dot{\phi}^2}{4f_\phi^2} + \frac{m_\phi^2}{2}. \quad (18)$$

For this estimate, we have neglected the finite- T contributions to the potential, as they quickly become subdominant to the zero- T part after the onset of ALP oscillations. Hence, the mode that experiences the fastest growth is

$$\left(\frac{k_{\text{peak}}}{a} \right)^2 = \frac{\dot{\phi}^2}{4f_\phi^2} \approx \frac{m_\phi^2}{2} (1 - \cos(\theta_i)). \quad (19)$$

In the second step, we have assumed that the initial ALP potential energy is converted into kinetic energy, again neglecting the finite- T contribution to the ALP potential. For $\theta_{\text{rel}} \sim \mathcal{O}(1)$, the maximum growth rate reads [28, 38]

$$\frac{\omega_{\text{max}}}{a} \approx \frac{m_\phi}{4}. \quad (20)$$

Modes within the instability band are then exponentially amplified,

$$u_k \propto \exp\left(\sqrt{\omega_{\text{max}}^2 - (k - k_{\text{peak}})^2} \tau\right), \quad (21)$$

eventually leading to the fragmentation of the ALP. For a given set of input parameters, we solve eqs. (16) and (17) numerically and extract the time evolution of the mode functions. The results of a benchmark simulation can be found in the appendix. In the following, we derive the necessary conditions for resonant growth to be efficient.

Conditions for efficient growth

To have ALP fragmentation, we need to ensure that ALP fluctuations occur in the first place. This implies

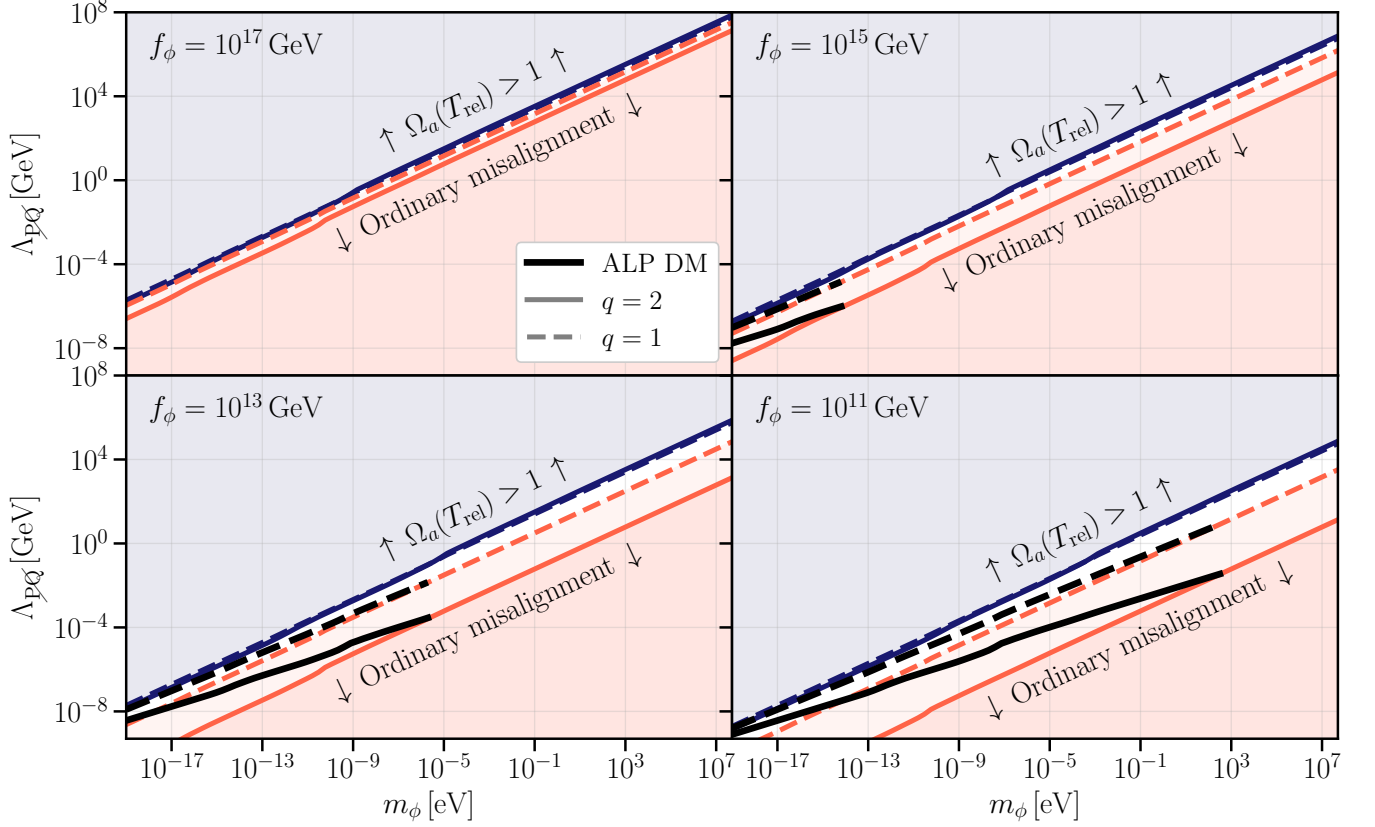


FIG. 2. Viable parameter space for ALP fragmentation in the $m_\phi - \Lambda_{\text{PQ}}$ parameter space. Each panel corresponds to a different choice of the ALP decay constant, $f_\phi \in \{10^{11}, 10^{13}, 10^{15}, 10^{17}\}$ GeV. Solid (dashed) lines employ $q = 2$ ($q = 1$), while the black lines indicate the parameter space where the correct CDM abundance is produced. In the blue-shaded region, the trapping period becomes too extended such that the ALP overcloses the Universe at the onset of oscillations. In the orange-shaded regime, the setup reduced to ordinary misalignment, where fragmentation is inefficient (cf. eq. (30)). Generally, smaller f_ϕ and larger q open up the viable parameter in terms of Λ_{PQ} . In addition, large decay constants severely limit the mass range where the ALP can be CDM.

a bound on the initial misalignment angle, which is required to be within the concave part of ALP potential,

$$|\theta_{\text{rel}}| > \frac{\pi}{2}. \quad (22)$$

If $|\theta_{\text{rel}}| < \pi/2$, the ALP would smoothly shift to the true minimum [10]. Via eq. (9), this can be translated into a bound on the phase shift δ between the two contributions to the potential (3).

The energy density of the fluctuations grows as $\rho_{\delta\phi} \propto \exp(2|\omega|\tau)$. For amplification to be cosmologically efficient, the growth rate has to exceed the Hubble rate, i.e.,

$$m_\phi \gtrsim H. \quad (23)$$

If this was not the case, the fluctuations would be overdamped (cf. eq. (17)). In the ordinary misalignment mechanism, the onset of ALP oscillations is defined by $m_\phi \sim H$. Then, amplification of unstable ALP modes can barely keep up with the expansion rate of the Universe. Even if the initial misalignment angle fulfills

eq. (22), cosmic expansion, $\dot{\phi}^2 \propto (a_{\text{osc}}/a)^3$, quickly shifts the instability band (18) into the IR. This shuts off the amplification of the initially unstable ALP modes, and ALP fragmentation becomes cosmologically inefficient. Therefore, we exclude the region where the thermal barrier in eq. (3) vanishes above $T_{\text{osc}}^{\text{mis}}$.

If trapping is effective, the Hubble parameter at the onset of oscillations decreases with respect to the conventional misalignment scenario. Then, $m_\phi > H_{\text{rel}}$ is always fulfilled, with ALP amplification becoming increasingly efficient as the trapping period is extended. We are interested in the case where the exponential resonance can convert the entire initial energy density of the zero mode into fluctuations. To obtain a rough estimate when this occurs, we again neglect the finite- T contributions to the potential. We employ $\rho_{\phi, \text{osc}} \sim m_\phi^2 f_\phi^2$ for the zero mode and

$$\rho_{\delta\phi} = \frac{1}{2a^2} \int \frac{d^3k}{(2\pi)^3} (k^2 |u_k|^2 + |u'_k|^2) \approx \frac{k_{\text{peak}}^4}{a_{\text{osc}}^4 (4\pi)^2}, \quad (24)$$

to estimate the initial fluctuation energy density. By imposing $k_{\text{peak}}/a_{\text{osc}} \sim m_\phi$ and $\rho_{\delta\phi} \propto \exp(m_\phi t/2)$, we can compute the elapsed cosmic time until $\rho_{\delta\phi} \sim \rho_{\phi,\text{osc}}$,

$$t \sim 2m_\phi^{-1} \ln \left(16\pi^2 \frac{f_\phi^2}{m_\phi^2} \right), \quad (25)$$

translating to

$$\frac{a_\star}{a_{\text{osc}}} \approx 1 + \frac{2H_{\text{osc}}}{m_\phi} \ln \left(16\pi^2 \frac{f_\phi^2}{m_\phi^2} \right). \quad (26)$$

To estimate the time when the resonant behavior shuts off, we compute the scale factor at which the largest initially unstable k -mode with $(k_{\text{max}}/a_{\text{osc}})^2 \sim 3m_\phi^2/2$ is shifted out of the instability band. Since the fluctuations are produced predominantly with $k \lesssim m_\phi$, we assume a matter-like scaling $k/a \propto \dot{\phi}^2 \propto a^{-3}$, such that

$$\left(\frac{k_{\text{max}}}{a_{\text{osc}}} \right)^2 \left(\frac{a_{\text{osc}}}{a_{\text{close}}} \right)^3 = \frac{m_\phi^2}{2}, \quad (27)$$

which gives

$$\frac{a_{\text{close}}}{a_{\text{osc}}} \sim 3^{\frac{1}{3}}. \quad (28)$$

Note that while this result neglects variations of the misalignment angle, it provides an informative criterion on the parameter space that allows for fragmentation. We demand $a_\star < a_{\text{close}}$, which yields

$$\frac{m_\phi}{2H_{\text{osc}}} \gtrsim (3^{\frac{1}{3}} - 1)^{-1} \ln \left(16\pi^2 \frac{f_\phi^2}{m_\phi^2} \right). \quad (29)$$

Hence, for typical values of the ALP mass and decay constant, we find

$$\frac{m_\phi}{H_{\text{osc}}} \gtrsim \mathcal{O}(500), \quad (30)$$

which we have also verified numerically. This condition can then be translated to a lower bound on the duration of the trapping period, mainly controlled by Λ_{PQ} .

For a consistent cosmological evolution, it is crucial to check that the ALP does not overclose the Universe at the onset of oscillations. Since we only consider the regime where the ALP is cosmologically stable, overclosure would necessarily lead to a matter-dominated Universe. Therefore, we exclude the parameter space where

$$\rho_\phi(T_{\text{osc}}) \approx m_\phi^2 f_\phi^2 (1 - \cos(\theta_i)) > \frac{\pi^2}{30} g_{\text{osc}} T_{\text{osc}}^4 = \rho_r(T_{\text{osc}}), \quad (31)$$

with ρ_r being the energy density of the primordial plasma.

An overview of the $m_\phi - \Lambda_{\text{PQ}}$ parameter space is shown in fig. 2 for different decay constants f_ϕ . We employ

$\delta = 0.01$; varying δ in the range $[0, \pi)$ has a negligible impact on the parameter space. The blue- and orange-shaded regions display the regions where the ALP overcloses the Universe and where the setup reduces to ordinary misalignment, respectively. Here, the dashed (straight) line corresponds to $q = 1$ ($q = 2$). In the region enclosed by the orange and blue lines, ALP fragmentation is possible, given eq. (29) is fulfilled. Note that for larger q , the range of possible $U(1)_{\text{PQ}}$ symmetry-breaking scales Λ_{PQ} increases. This is because of the modified temperature dependence of the second term in eq. (3), requiring larger shifts of Λ_{PQ} to achieve a given release temperature.

Relic abundance

In the following, we derive the relic ALP abundance $\Omega_{\phi,0}$ as a function of the model parameters, and identify the parameter space where the ALP can constitute all of CDM, i.e., $h^2 \Omega_{\phi,0} = 0.12$ [75].

From the onset of oscillations, the ALP zero mode follows a matter-like scaling, $\rho_\phi \sim a^{-3}$, while amplifying fluctuations whose energy density eventually becomes comparable, $\rho_{\delta\phi} \sim \rho_\phi$. The ALP quanta are dominantly produced with momenta below the ALP mass $k/a \lesssim m_\phi(\theta_i) \sim m_\phi$ (cf. eq. (19)), hence are non-relativistic from the moment of production. Therefore, we can estimate the total relic ALP abundance as

$$\rho_{\phi,0} = \rho_\phi(T_{\text{osc}}) \left(\frac{a_{\text{osc}}}{a_0} \right)^3, \quad (32)$$

where T_{osc} is given by eq. (11) and a_0 is the scale factor today. This can be expressed in terms of the critical energy density as

$$h^2 \Omega_{\phi,0} = \Omega_\phi(T_{\text{osc}}) \left(\frac{a_{\text{osc}}}{a_0} \right)^3 \left(\frac{H_{\text{osc}}}{H_{100}} \right)^2, \quad (33)$$

with $H_{100} = 100 \text{ km}/(\text{Mpc s})$. Employing the Hubble parameter at the onset of rolling (12), we have

$$\Omega_\phi(T_{\text{osc}}) = \left(\frac{f_\phi^2 (1 - \cos(\theta_i))}{3M_{\text{Pl}}^2} \right) \left(\frac{T_{\text{osc}}^{\text{mis}}}{T_{\text{osc}}} \right)^4 \left(\frac{g_{\text{mis}}}{g_{\text{osc}}} \right). \quad (34)$$

Hence, a finite trapping period enhances the relative ALP abundance, while $T_{\text{osc}} = T_{\text{osc}}^{\text{mis}}$ recovers the standard expression for ALP misalignment.

Expressing the scale factor ratio in eq. (33) by temperature we find

$$h^2 \Omega_{\phi,0} = \frac{f_\phi^2}{3M_{\text{Pl}}^2} (1 - \cos(\theta_i)) \left(\frac{T_0}{T_{\text{osc}}} \right)^3 \left(\frac{m_\phi}{H_{100}} \right)^2 \frac{g_0}{g_{\text{osc}}}, \quad (35)$$

where we have used that $H_{\text{osc}} = m_\phi(T_{\text{osc}}/T_{\text{osc}}^{\text{mis}})^2$. Lower T_{osc} , i.e., longer trapping, induces a larger present-day ALP abundance. Via eq. (11), this can be rewritten as follows:

$$h^2\Omega_{\phi,0} \simeq \begin{cases} 4 \times 10^{-2} g_\star^{-1} C_1(\delta) \left(\frac{\Lambda_{\cancel{PQ}}}{\text{GeV}}\right)^9 \left(\frac{\text{eV}}{m_\phi}\right)^4 \left(\frac{10^{12} \text{ GeV}}{f_\phi}\right)^4, & q = 1, \\ 5 \times 10^6 g_\star^{-1} C_2(\delta) \left(\frac{\Lambda_{\cancel{PQ}}}{\text{GeV}}\right)^3 \left(\frac{\text{eV}}{m_\phi}\right) \left(\frac{10^{12} \text{ GeV}}{f_\phi}\right), & q = 2. \end{cases} \quad (36)$$

Here, we have specialized to the cases $q \in \{1, 2\}$. The dependence on the initial misalignment angle, or equivalently, on δ , is captured by

$$C_1(\delta) = (1 - \cos \theta_i) \left(\frac{\cos(2\theta_i + \delta)}{-\cos(\theta_i)} \right)^3, \quad (37)$$

$$C_2(\delta) = (1 - \cos \theta_i) \left(\frac{\cos(2\theta_i + \delta)}{-\cos(\theta_i)} \right)^{\frac{3}{2}}. \quad (38)$$

For a set of model parameters $\{m_\phi, f_\phi, \delta\}$, $\Lambda_{\cancel{PQ}}$ can be adjusted within the limits derived in the last section to meet today's CDM density. Note that larger q generally requires a smaller $\Lambda_{\cancel{PQ}}$ to achieve a given relic abundance.

By the black lines in fig. 2, we indicate the parameter combinations where $h^2\Omega_{\phi,0} = 0.12$ is fulfilled. The dashed (solid) line again corresponds to $q = 1$ ($q = 2$). In the ordinary misalignment mechanism, the relic abundance becomes independent of $\Lambda_{\cancel{PQ}}$. Therefore, the black curves intersect with the orange lines at the mass where the correct ALP abundance is reproduced without trapping. Moving to smaller ALP masses, the standard misalignment mechanism would underproduce CDM. Therefore, a finite trapping period is required to enhance the ALP abundance. As a consequence, larger ratios $\Lambda_{\cancel{PQ}}/m_\phi$ are necessary, and the black lines approach the overclosure bounds.

Smaller f_ϕ generally allow for a wider range of ALP masses due to the suppression of the ALP energy density (cf. eq. (34)). For, e.g., $f_\phi = 10^{17} \text{ GeV}$, we cannot reproduce the required CDM abundance in the chosen mass range. In the next section, we will see that the GW signal is suppressed for small f_ϕ , limiting the parameter space where both sizable GW amplitudes and the correct CDM abundance is achieved. This is a well-known problem in theories featuring ALP-induced GWs [27, 31, 64, 66]. Note, however, that the large- m_ϕ parameter space can be opened up through additional model building, e.g., by considering a time-varying ALP mass [76–81] or a period of kination [31].

GRAVITATIONAL WAVES

The resonant production of ALP quanta generates anisotropies in the energy momentum tensor of the cosmic fluid, i.e., leading to the generation of stochastic GWs [29, 31]. In the following, we first provide simple scaling estimates of the position of the spectral peak,

before discussing our numerical computation and the associated observational prospects.

Analytic estimates

The amplitude of a SGWB can generally be estimated as [31, 42, 64, 65, 82]

$$\Omega_{\text{GW},\star}^{\text{peak}} \simeq \Omega_{\text{src}}^2 \left(\frac{a_\star H_\star}{k_{\text{peak}}} \right)^2 \simeq \left(\frac{\Omega_{\phi,\star}}{2} \right)^2 \left(\frac{a_\star H_\star}{k_{\text{peak}}} \right)^2. \quad (39)$$

Here, $\Omega_{\text{src}} \simeq \Omega_{\phi,\star}/2$ denotes the energy budget of the source, which corresponds to the ALP energy density at the time of GW production. We have included a factor $1/2$, since the initial ALP energy density is transferred to both kinetic and gradient energy, however, only the gradient contribution acts as a GW source. The second term amounts to a suppression factor that depends on the typical scale of the produced GWs; fluctuations on larger spatial scales induce stronger anisotropies, hence enhance the GW amplitude. Note that for fragmentation to be efficient, the growth rate has to exceed the Hubble parameter by orders of magnitude (cf. eq. (30)). Therefore, ALP production takes place within a fraction of a Hubble time, and we evaluate all quantities that enter eq. (39) at the onset of oscillations. Then, the characteristic physical momentum scale is given by the mode which experiences the fastest growth,

$$\frac{k_{\text{peak}}}{a} \simeq \frac{m_\phi}{\sqrt{2}} (1 - \cos \theta_i)^{\frac{1}{2}}. \quad (40)$$

Employing eq. (12), we then express the ratio of the Hubble rate and the physical peak momentum as

$$\left(\frac{a_{\text{osc}} H_{\text{osc}}}{k_{\text{peak}}} \right)^2 = 2(1 - \cos \theta_i) \left(\frac{T_{\text{osc}}}{T_{\text{mis}}^{\text{osc}}} \right)^4 \frac{g_{\text{osc}}}{g_{\text{mis}}}, \quad (41)$$

where $T_{\text{osc}}^{\text{mis}}$ is given by eq. (2). The relative ALP energy density at the time of oscillations is given by eq. (34). Specializing again to the cases $q \in \{1, 2\}$ and evaluating eq. (39) yields

$$\Omega_{\text{GW},\star}^{\text{peak}} \simeq \begin{cases} 65 g_{\text{osc}}^{-1} C_3 \left(\frac{\Lambda_{\cancel{PQ}}^6}{M_{\text{Pl}} f_\phi^2 m_\phi^3} \right)^2, & q = 1, \\ 4 g_{\text{osc}}^{-1} C_4 \left(\frac{\Lambda_{\cancel{PQ}}^2}{m_\phi M_{\text{Pl}}} \right)^2, & q = 2, \end{cases} \quad (42)$$

with

$$C_3 = \left(\frac{\sqrt{2}(1 - \cos \theta_i)^{\frac{1}{2}} \cos^2(2\theta_i + \delta)}{\cos^2(\theta_i)} \right)^2, \quad (43)$$

$$C_4 = \left(\frac{\sqrt{2}(1 - \cos(\theta_i))^{\frac{1}{2}} \cos(2\theta_i + \delta)}{\cos \theta_i} \right)^2. \quad (44)$$

This allows for a direct estimate of the anticipated GW amplitude given some benchmark parameters $\{m_\phi, f_\phi, \Lambda_{\text{PQ}}\}$. However, note that the model parameters are not independent of each other, but have to be adjusted in order to remain within the viable region of parameter space. Decreasing m_ϕ and f_ϕ , for instance, requires a smaller $U(1)_{\text{PQ}}$ breaking scale Λ_{PQ} for the axion to not overclose the Universe.

Numerical computation

Employing our numerical analysis of eqs. (16) and (17), we can directly compute the resulting GW spectrum from the simulated mode functions u_k . The spectral GW energy density from scalar field fluctuations reads [31, 43]

$$\begin{aligned} \frac{d\Omega_{\text{GW},*}}{d \log k} &= \frac{1}{\rho_{\text{tot}}} \left(\frac{k}{4\pi^2 a_\star^2 M_{\text{Pl}}} \right)^2 \int_0^\infty dq q^5 \sin^4 \theta \\ &\times \int_{|k-q|}^{|k+q|} dl l \left[|I_c(\mathbf{k}, \mathbf{q}, \tau)|^2 + |I_s(\mathbf{k}, \mathbf{q}, \tau)|^2 \right], \end{aligned} \quad (45)$$

where ρ_{tot} denotes the total energy density in the Universe at the time of production. Furthermore,

$$l = |\mathbf{k} - \mathbf{q}| = \sqrt{k^2 - q^2 - 2kq \cos \theta}, \quad (46)$$

and the time integrals over the mode functions are given by

$$I_{c/s}(\mathbf{k}, \mathbf{q}, \tau) = \int_{\tau_{\text{osc}}}^{\tau_\star} \frac{d\eta}{a(\eta)} \left\{ \begin{array}{l} \cos(k\eta) \\ \sin(k\eta) \end{array} \right\} u_q(\eta) u_l(\eta). \quad (47)$$

For the computation we follow the strategy from [31]. That is, we discretize the integrals into sums over the simulated mode functions. Finally, to obtain the GW spectra today, we redshift via [48, 49]

$$h^2 \Omega_{\text{GW},0} = 1.67 \times 10^{-5} \left(\frac{100}{g_\star} \right)^{\frac{1}{3}} \Omega_{\text{GW},*}, \quad (48)$$

$$f_0 = 1.65 \times 10^{-7} \text{ Hz} \frac{k}{a_\star H_\star} \frac{T_\star}{\text{GeV}} \left(\frac{g_\star}{100} \right)^{\frac{1}{6}}. \quad (49)$$

Results

In fig. 3, we show some exemplary GW spectra, computed numerically with the benchmark parameters given in table I. The colored areas indicate the power-law integrated sensitivity curves [83, 84] of the future Square Kilometre Array (SKA) [85], μARES [86], Big Bang Observer (BBO) [87], and LISA [88–90]. In addition, we display the projected prospects for GW detection via Lunar Laser Ranging (LLR) [91].

The spectra plotted with solid lines correspond to benchmarks where the ALP reproduces the observed CDM abundance, $h^2 \Omega_{\phi,0} = 0.12$. The red stars correspond to our estimates of the peak position (42). Note that our analytic results slightly overestimate the peak frequency and amplitude. This is because we evaluate all quantities at the onset of oscillations, i.e., neglect their redshift until the time of GW production. In addition, our simulations show that the factor 1/2 in eq. (39) overestimates the gradient contribution to the total fluctuation energy density.

By combining eqs. (36) and (42), the condition to obtain the correct relic abundance can be translated to the $f - h^2 \Omega_{\text{GW},0}$ parameter space; this is indicated by the gray dotted line. Above this line, ALPs are overproduced. Hence, we do not find a parameter space that yields both detectable GW signals and ALP CDM. This generic feature of fragmentation models was already noted in [29, 31] and can be understood from eq. (39) and the scaling behavior of the ALP. From the moment of production, the ALP quanta redshift like matter, hence are enhanced $\propto a$ compared to the background. A larger GW frequency, i.e., an earlier onset of ALP oscillations therefore requires a smaller initial relative ALP energy density to not overclose the Universe, decreasing the GW amplitude.

In the remaining parameter space, further model building is required to suppress the relic ALP abundance. However, it is useful to study this region to obtain, for instance, information on the maximum GW amplitude. Increasing the ALP mass shifts the GW spectra to higher frequencies. The amplitude is determined by the combination of f_ϕ and Λ_{PQ} . Our peak estimate correctly captures the scaling behavior of the signal. Interestingly, we find maximum amplitudes of $h^2 \Omega_{\text{GW},0} \sim \mathcal{O}(10^{-12})$, exceeding the findings from previous studies of fragmentation-induced GW signals [29, 31] by roughly two orders of magnitude. This is caused by delayed onset of ALP oscillations, which increases the energy budget available to be converted into GWs.³ Notably, we find a change of the spectral behavior around the peak, where

³ See also [27] for a similar enhancement of the GW signal from axion-photon systems.

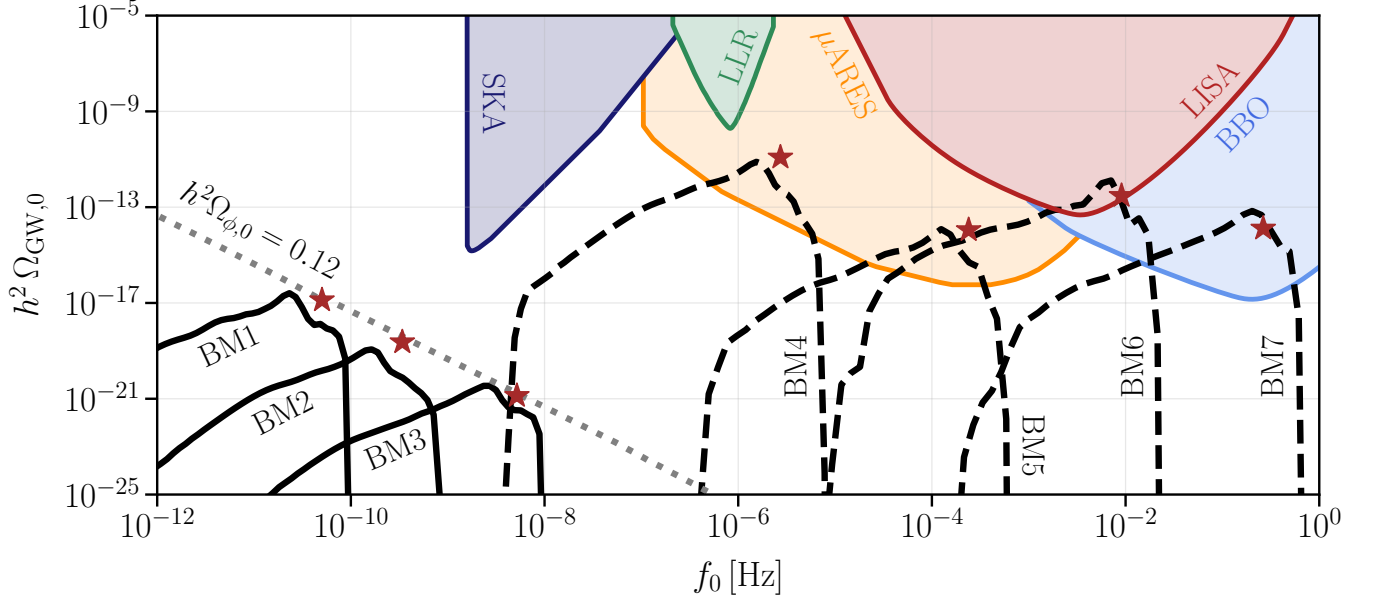


FIG. 3. Projected present GW spectra for the benchmark parameters from table I. The colored curves indicate the power-law integrated sensitivities of several future GW experiments. The black solid lines correspond to benchmarks that reproduce the correct CDM abundance. That is, ALPs are overproduced above the gray dotted line and the dashed spectra can only be realized through further model building to suppress the relic abundance. By varying the ALP mass and decay constants, the spectral peak moves into the sensitivity regions of future observatories. The red star indicates our analytic estimate of the peak (42), which correctly describes the scaling behavior of the GW signal.

	m_ϕ [eV]	f_ϕ [GeV]	$\Lambda_{\cancel{B\bar{B}}}$ [GeV]	δ	q
BM1	10^{-19}	10^{14}	7.5×10^{-9}	1	2
BM2	10^{-17}	5×10^{13}	3.1×10^{-8}	0.1	2
BM3	10^{-15}	10^{13}	7.6×10^{-8}	1	2
BM4	10^{-9}	5×10^{15}	0.048	0.1	1
BM5	10^{-5}	10^{15}	1.2	0.01	2
BM6	10^{-2}	2×10^{15}	100	0.3	2
BM7	10	10^{15}	1980	0.1	1

TABLE I. Benchmark parameters employed for the GW spectra in fig. 3.

$h^2 \Omega_{\text{GW},0} \propto k^2$, compared to ref. [31]. In addition, our spectra are peaked towards the UV, which differs from the IR-dominated signals found in [29]. Hence, the finite-temperature contributions to the ALP potential directly affect the form of the GW signal. However, our linearized analysis is not sufficient to make conclusive statements, as higher-order interactions between the ALP quanta alter the spectral shape. This requires a lattice analysis, which is relegated to future work.

DISCUSSION AND CONCLUSIONS

In this work, we have investigated the generation of a SGWB through ALP fragmentation in finite-temperature trapped misalignment models. Below, we summarize our key findings, discuss their broader implications, and outline directions for future work.

We have shown that explicit PQ breaking through finite-temperature contributions to the potential traps the axion field in a metastable minimum. Once the thermal barrier disappears, the field is released and undergoes rapid oscillations around the true minimum. The finite ALP velocity triggers a resonance in the equation of motion, leading to the amplification of long-wavelength fluctuations. If the trapping period is sufficiently long, the resulting field fragmentation produces a GW background analogous to that from conventional axion fragmentation [29, 31], along with an inhomogeneous axion field population. Our analytic estimates and numerical analysis show that the GW amplitude is enhanced by up to two orders of magnitude relative to the standard fragmentation case. This is a direct consequence of the delayed onset of oscillations; the GW amplitude grows with the length of the trapping period. The GW peak frequency is mainly determined by the ALP mass m_ϕ . The enhancement of the amplitude implies that the GWs are within the reach of future interferometers such as LISA, BBO, and μAres , as well as pulsar timing arrays (see

fig. 3). However, this requires an additional mechanism to suppress the relic ALP abundance.

The spectral shape displays a k^2 scaling around the peak, which changes to k^3 in the IR before the rapid falloff. Our signal peaks in the UV, whereas previous works found an IR-dominated peak in the ALP monodromy scenario [29]. This reveals that the GW spectra are sensitive to the release dynamics and the shape of the finite-temperature potential. These spectral features of the GWs may provide a discriminant between different ALP-induced GW signals.

Finally, we comment on future directions based on the findings of this work. Our linearized analysis describes the main qualitative features of the ALP dynamics, however, a complete nonlinear treatment is required to conclude these predictions.⁴ Lattice simulations of the post-release dynamics include mode-mode couplings, which induce spectral broadening. Capturing these nonlinear effects along with the backreaction of amplified modes on the zero mode provides a quantitative prediction of the GW spectrum.

Considering the QCD axion, where temperature-dependent instanton effects may induce similar trapping dynamics, is a natural extension. Furthermore, one may adopt other trapping potentials arising from, for instance, interactions with a dark pure Yang-Mills sector, employing the free energy calculated in [93]. These types of dark sectors are often realized in string theory-inspired axion models within the axiverse. Such axion models have also been proposed as a framework for realizing high-quality QCD axions; see, for instance, [94].

Lastly, since most of the parameter space is constrained by the CDM abundance in the minimal setup, it would be interesting to explore potential mechanisms to alleviate the overproduction of ALPs. One example was suggested in [29], which considers an additional relativistic phase after ALP fragmentation to dilute the relic ALP abundance.

In summary, the resonant behavior emerging from thermally trapped misalignment represents a robust mechanism for generating SGWBs in the early Universe. The distinctive spectral features and amplitude enhancements found here motivate future theoretical, numerical, and observational efforts to probe the rich dynamics of axion-like sectors through their gravitational-wave signatures.

Acknowledgements. We thank Dieter B. in Mainz that initially sparked this work. We further thank C. Gerlach, E. Morgante, W. Ratzinger, and P. Schwaller for comments and discussion of the manuscript. NR thanks P. Sørensen for illuminating him into thinking

about trapped axions. NR acknowledges support in part by the European Union - NextGenerationEU through the PRIN Project “Charting unexplored avenues in Dark Matter” (20224JR28W), and INFN TAsP.

APPENDIX

In this section, we discuss our numerical approach to solving the ALP equations of motion.

Solving the equations of motion

Given a set of input parameters $\{m_\phi, f_\phi, \Lambda_{\text{PQ}}, \delta, n, q\}$, we solve the coupled eqs. (16) and (17) numerically for $N_k = 10^4$ ALP modes. The result for a benchmark that reproduces the correct CDM abundance is shown in fig. 4. Here, the upper panel displays the relative energy density of the zero mode and the fluctuations, while the second panel shows the oscillation amplitude. Initially, the energy density of the zero mode is merely affected by the cosmic expansion, i.e. $\Omega_\phi \propto a$. During each oscillation cycle, unstable modes receive an amplification, increasing the fluctuation energy density which eventually becomes comparable to that of the zero mode, $\Omega_{\delta\phi} \sim \Omega_\phi$. For the given benchmark this occurs at $a \approx 1.37a_{\text{osc}}$. Subsequently, backreaction from the produced quanta on the zero mode becomes important, governed by the third derivative of the potential in eq. (16). We observe that this leads to an oscillating behavior of the energy densities (cf. upper panel). As the zero-mode energy density decreases upon the impact of the fluctuations, the oscillation amplitude decreases (cf. lower panel). This slows down the zero mode; i.e., the instability band becomes narrower and eventually vanishes.

Note that once the fluctuations grow large, our perturbative approach necessarily induces uncertainties as the expansion (15) breaks down. Higher-order effects that are not captured by our simulation, such as interactions between the produced ALP quanta, become important. To this end, classical lattice simulations are required [29], which is beyond the scope of our work.

Fig. 5 shows the associated energy spectra of the fluctuations and GWs at different times during the simulation, as a function of the physical momentum normalized to the Hubble parameter at the start of the simulation. The GW spectrum is computed numerically from the extracted mode functions, as described in the main body. GWs are predominantly produced during the initial stages of the evolution, as shown by the red benchmark in the lower panel. This benchmark approximately corresponds to the moment where backreaction sets in, which, however, has a minor impact on the GW spectrum. On the lattice, where the full backreaction is incorporated, the GW spectrum typically broadens due to in-

⁴ Recent lattice study of \mathcal{Z}_N QCD axions [92], which was one of the original model motivations for trapped misalignment, affirms the necessity of simulations.

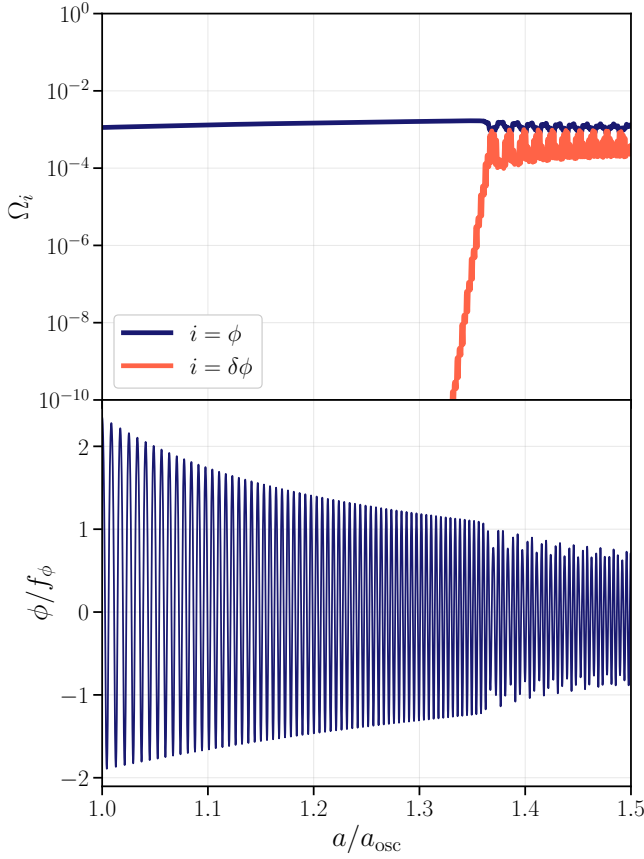


FIG. 4. Exemplary simulation of the fragmentation process, employing $m_\phi = 10^{-19}$ eV, $f_\phi = \Lambda_{\text{PQ}} \approx 7.5 \times 10^{-9}$ GeV, $\delta = 1$, $n = 2$, and $q = 2$. Top: Energy densities of the zero mode (blue) and the fluctuations (orange), normalized to the total energy density of the Universe, as a function of the scale factor. Bottom: Oscillation amplitude of the zero mode. Around $a \approx 1.36a_{\text{osc}}$, the fluctuation energy density becomes comparable to the one of the zero mode. Then, backreaction sets in and dampens the oscillations.

interactions among the modes. As we are mostly interested in estimating the position of the resulting GW peak, we consider our results robust. Finally, let us point out the remarkable agreement between the numerical computation and the analytical estimate of the GW peak frequency (eq. (40)), and amplitude (eq. (42)), indicated by the orange star in the lower panel.

* nramberg@sissa.it

† dschmitt@itp.uni-frankfurt.de

- [1] R. D. Peccei and H. R. Quinn, Phys. Rev. Lett. **38**, 1440 (1977).
- [2] F. Wilczek, Phys. Rev. Lett. **40**, 279 (1978).
- [3] S. Weinberg, Phys. Rev. Lett. **40**, 223 (1978).
- [4] J. Preskill, M. B. Wise, and F. Wilczek, Phys. Lett. B **120**, 127 (1983).

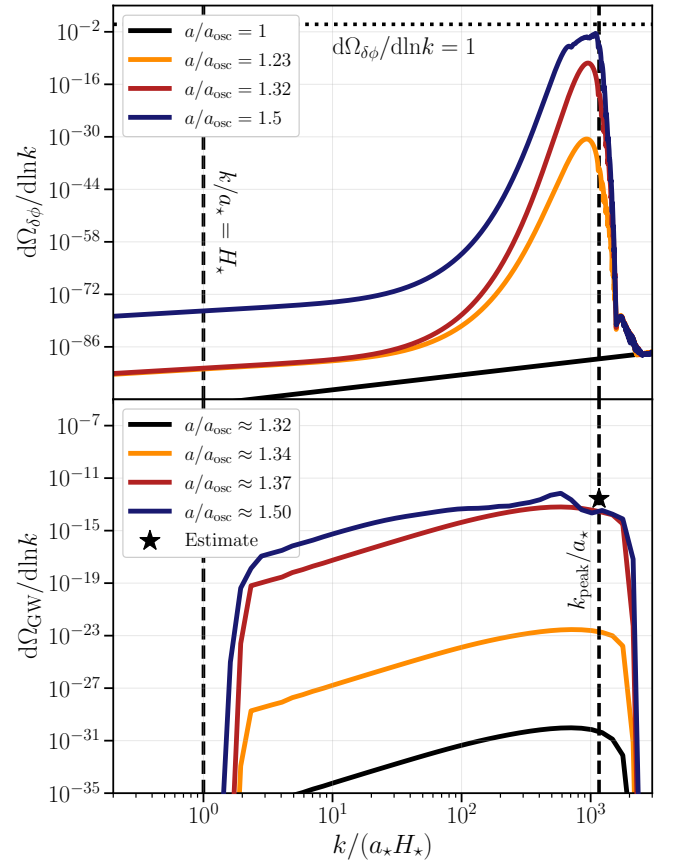


FIG. 5. Spectral ALP (top) and GW (bottom) energy density at different times during the simulation, using the model parameters from fig. 4. We display the spectra as a function of the physical momenta k/a_* , normalized to the Hubble rate at the time of production. The dashed line in the UV corresponds to our estimate of the fastest growing mode (19), which also sets the peak of the GW spectrum.

- [5] L. F. Abbott and P. Sikivie, Phys. Lett. B **120**, 133 (1983).
- [6] M. Dine and W. Fischler, Phys. Lett. B **120**, 137 (1983).
- [7] S. Nakagawa, F. Takahashi, and M. Yamada, JCAP **05**, 062 (2021), arXiv:2012.13592 [hep-ph].
- [8] L. Di Luzio, B. Gavela, P. Quilez, and A. Ringwald, JCAP **10**, 001 (2021), arXiv:2102.01082 [hep-ph].
- [9] L. Di Luzio, B. Gavela, P. Quilez, and A. Ringwald, JHEP **05**, 184 (2021), arXiv:2102.00012 [hep-ph].
- [10] L. Di Luzio and P. Sørensen, JHEP **10**, 239 (2024), arXiv:2408.04623 [hep-ph].
- [11] A. Hook, Phys. Rev. Lett. **120**, 261802 (2018), arXiv:1802.10093 [hep-ph].
- [12] M. Gorghetto, E. Hardy, and G. Villadoro, SciPost Phys. **10**, 050 (2021), arXiv:2007.04990 [hep-ph].
- [13] J. N. Benabou, M. Buschmann, J. W. Foster, and B. R. Safdi, Phys. Rev. Lett. **134**, 241003 (2025), arXiv:2412.08699 [hep-ph].
- [14] K. Saikawa, J. Redondo, A. Vaquero, and M. Kaltschmidt, JCAP **10**, 043 (2024), arXiv:2401.17253 [hep-ph].
- [15] J. Correia, M. Hindmarsh, J. Lizarraga, A. Lopez-

- Eiguren, K. Rummukainen, and J. Urrestilla, Phys. Rev. D **111**, 063532 (2025), arXiv:2410.18064 [hep-ph].
- [16] P. Svrcek and E. Witten, JHEP **06**, 051 (2006), arXiv:hep-th/0605206.
- [17] A. Arvanitaki, S. Dimopoulos, S. Dubovsky, N. Kaloper, and J. March-Russell, Phys. Rev. D **81**, 123530 (2010), arXiv:0905.4720 [hep-th].
- [18] D. J. E. Marsh, Phys. Rept. **643**, 1 (2016), arXiv:1510.07633 [astro-ph.CO].
- [19] J. E. Kim, Phys. Rept. **150**, 1 (1987).
- [20] K. Freese, J. A. Frieman, and A. V. Olinto, Phys. Rev. Lett. **65**, 3233 (1990).
- [21] E. Pajer and M. Peloso, Class. Quant. Grav. **30**, 214002 (2013), arXiv:1305.3557 [hep-th].
- [22] P. Adshead, J. T. Giblin, T. R. Scully, and E. I. Sfakianakis, JCAP **12**, 034 (2015), arXiv:1502.06506 [astro-ph.CO].
- [23] R. Daido, F. Takahashi, and W. Yin, JCAP **05**, 044 (2017), arXiv:1702.03284 [hep-ph].
- [24] F. Takahashi and W. Yin, JCAP **10**, 057 (2021), arXiv:2105.10493 [hep-ph].
- [25] V. Domcke, Y. Ema, and K. Mukaida, JHEP **02**, 055 (2020), arXiv:1910.01205 [hep-ph].
- [26] N. Kitajima, S. Nakagawa, and F. Takahashi, Phys. Rev. D **105**, 103011 (2022), arXiv:2111.06696 [hep-ph].
- [27] C. Gerlach, D. Schmitt, and P. Schwaller, (2025), arXiv:2504.05386 [hep-ph].
- [28] N. Fonseca, E. Morgante, R. Sato, and G. Servant, JHEP **04**, 010 (2020), arXiv:1911.08472 [hep-ph].
- [29] A. Chatrchyan and J. Jaeckel, JCAP **02**, 003 (2021), arXiv:2004.07844 [hep-ph].
- [30] E. Morgante, W. Ratzinger, R. Sato, and B. A. Stefanek, JHEP **12**, 037 (2021), arXiv:2109.13823 [hep-ph].
- [31] E. Madge, W. Ratzinger, D. Schmitt, and P. Schwaller, SciPost Phys. **12**, 171 (2022), arXiv:2111.12730 [hep-ph].
- [32] C. Eröncel and G. Servant, JCAP **01**, 009 (2023), arXiv:2207.10111 [hep-ph].
- [33] C. Eröncel, R. Sato, G. Servant, and P. Sørensen, JCAP **10**, 053 (2022), arXiv:2206.14259 [hep-ph].
- [34] A. Chatrchyan, C. Eröncel, M. Koschnitzke, and G. Servant, JCAP **10**, 068 (2023), arXiv:2305.03756 [hep-ph].
- [35] P. B. Greene, L. Kofman, and A. A. Starobinsky, Nucl. Phys. B **543**, 423 (1999), arXiv:hep-ph/9808477.
- [36] L. Kofman, A. D. Linde, and A. A. Starobinsky, Phys. Rev. Lett. **73**, 3195 (1994), arXiv:hep-th/9405187.
- [37] P. B. Greene, L. Kofman, A. D. Linde, and A. A. Starobinsky, Phys. Rev. D **56**, 6175 (1997), arXiv:hep-ph/9705347.
- [38] L. Kofman, A. D. Linde, and A. A. Starobinsky, Phys. Rev. D **56**, 3258 (1997), arXiv:hep-ph/9704452.
- [39] J. F. Dufaux, A. Bergman, G. N. Felder, L. Kofman, and J.-P. Uzan, Phys. Rev. D **76**, 123517 (2007), arXiv:0707.0875 [astro-ph].
- [40] J.-F. Dufaux, G. Felder, L. Kofman, and O. Navros, JCAP **03**, 001 (2009), arXiv:0812.2917 [astro-ph].
- [41] J. L. Cook and L. Sorbo, Phys. Rev. D **85**, 023534 (2012), [Erratum: Phys. Rev. D **86**, 069901 (2012)], arXiv:1109.0022 [astro-ph.CO].
- [42] W. Buchmüller, V. Domcke, K. Kamada, and K. Schmitz, JCAP **10**, 003 (2013), arXiv:1305.3392 [hep-ph].
- [43] D. G. Figueroa and F. Torrenti, JCAP **10**, 057 (2017), arXiv:1707.04533 [astro-ph.CO].
- [44] D. G. Figueroa, A. Florio, F. Torrenti, and W. Valkenburg, JCAP **04**, 035 (2021), arXiv:2006.15122 [astro-ph.CO].
- [45] Y. Bea, J. Casallerrey-Solana, T. Giannakopoulos, A. Jansen, S. Krippendorff, D. Mateos, M. Sanchez-Garitaonandia, and M. Zilhão, (2021), arXiv:2112.15478 [hep-th].
- [46] D. Schmitt and L. Sagunski, JCAP **02**, 075 (2025), arXiv:2409.05851 [hep-ph].
- [47] T. P. Dutka, T. H. Jung, and C. S. Shin, JHEP **05**, 182 (2025), arXiv:2412.15864 [hep-ph].
- [48] C. Caprini and D. G. Figueroa, Class. Quant. Grav. **35**, 163001 (2018), arXiv:1801.04268 [astro-ph.CO].
- [49] M. Kamionkowski, A. Kosowsky, and M. S. Turner, Phys. Rev. D **49**, 2837 (1994), arXiv:astro-ph/9310044.
- [50] M. Hindmarsh, S. J. Huber, K. Rummukainen, and D. J. Weir, Phys. Rev. Lett. **112**, 041301 (2014), arXiv:1304.2433 [hep-ph].
- [51] P. Schwaller, Phys. Rev. Lett. **115**, 181101 (2015), arXiv:1504.07263 [hep-ph].
- [52] C. Caprini *et al.*, JCAP **03**, 024 (2020), arXiv:1910.13125 [astro-ph.CO].
- [53] D. Croon, O. Gould, P. Schicho, T. V. I. Tenkanen, and G. White, JHEP **04**, 055 (2021), arXiv:2009.10080 [hep-ph].
- [54] E. Morgante, N. Ramberg, and P. Schwaller, Phys. Rev. D **107**, 036010 (2023), arXiv:2210.11821 [hep-ph].
- [55] M. Kierkla, A. Karam, and B. Swiezewska, JHEP **03**, 007 (2023), arXiv:2210.07075 [astro-ph.CO].
- [56] L. Sagunski, P. Schicho, and D. Schmitt, Phys. Rev. D **107**, 123512 (2023), arXiv:2303.02450 [hep-ph].
- [57] M. Kierkla, B. Swiezewska, T. V. I. Tenkanen, and J. van de Vis, JHEP **02**, 234 (2024), arXiv:2312.12413 [hep-ph].
- [58] M. Kierkla, P. Schicho, B. Swiezewska, T. V. I. Tenkanen, and J. van de Vis, JHEP **07**, 153 (2025), arXiv:2503.13597 [hep-ph].
- [59] M. Kierkla, N. Ramberg, P. Schicho, and D. Schmitt, (2025), arXiv:2506.15496 [hep-ph].
- [60] M. M. Anber and L. Sorbo, Phys. Rev. D **85**, 123537 (2012), arXiv:1203.5849 [astro-ph.CO].
- [61] V. Domcke, M. Pieroni, and P. Binétruy, JCAP **06**, 031 (2016), arXiv:1603.01287 [astro-ph.CO].
- [62] A. Maleknejad, JHEP **07**, 104 (2016), arXiv:1604.03327 [hep-ph].
- [63] J. R. C. Cuissa and D. G. Figueroa, JCAP **06**, 002 (2019), arXiv:1812.03132 [astro-ph.CO].
- [64] C. S. Machado, W. Ratzinger, P. Schwaller, and B. A. Stefanek, JHEP **01**, 053 (2019), arXiv:1811.01950 [hep-ph].
- [65] C. S. Machado, W. Ratzinger, P. Schwaller, and B. A. Stefanek, Phys. Rev. D **102**, 075033 (2020), arXiv:1912.01007 [hep-ph].
- [66] W. Ratzinger, P. Schwaller, and B. A. Stefanek, SciPost Phys. **11**, 001 (2021), arXiv:2012.11584 [astro-ph.CO].
- [67] B. Salehian, M. A. Gorji, S. Mukohyama, and H. Firouzjahi, JHEP **05**, 043 (2021), arXiv:2007.08148 [hep-ph].
- [68] R. Namba and M. Suzuki, Phys. Rev. D **102**, 123527 (2020), arXiv:2009.13909 [astro-ph.CO].
- [69] T. Kite, A. Ravenni, S. P. Patil, and J. Chluba, Mon. Not. Roy. Astron. Soc. **505**, 4396 (2021), arXiv:2010.00040 [astro-ph.CO].
- [70] N. Kitajima, J. Soda, and Y. Urakawa, Phys. Rev. Lett. **126**, 121301 (2021), arXiv:2010.10990 [astro-ph.CO].
- [71] A. Banerjee, E. Madge, G. Perez, W. Ratzinger,

- and P. Schwaller, Phys. Rev. D **104**, 055026 (2021), arXiv:2105.12135 [hep-ph].
- [72] E. Madge, E. Morgante, C. Puchades-Ibáñez, N. Ramberg, W. Ratzinger, S. Schenk, and P. Schwaller, JHEP **10**, 171 (2023), arXiv:2306.14856 [hep-ph].
- [73] H. Su, B. Xu, J. Chen, C. Liu, and Y.-L. Zhang, (2025), arXiv:2503.20778 [astro-ph.CO].
- [74] N. W. McLachlan, *Theory and Application of Mathieu Functions* (Clarendon Press, Oxford, 1947) pp. xii+401, corrected republication by Dover Publications, Inc., New York, 1964.
- [75] N. Aghanim *et al.* (Planck), Astron. Astrophys. **641**, A6 (2020), [Erratum: Astron.Astrophys. 652, C4 (2021)], arXiv:1807.06209 [astro-ph.CO].
- [76] L. McAllister, E. Silverstein, and A. Westphal, Phys. Rev. D **82**, 046003 (2010), arXiv:0808.0706 [hep-th].
- [77] E. Silverstein and A. Westphal, Phys. Rev. D **78**, 106003 (2008), arXiv:0803.3085 [hep-th].
- [78] A. Hebecker, S. C. Kraus, and L. T. Witkowski, Phys. Lett. B **737**, 16 (2014), arXiv:1404.3711 [hep-th].
- [79] L. McAllister, E. Silverstein, A. Westphal, and T. Wrase, JHEP **09**, 123 (2014), arXiv:1405.3652 [hep-th].
- [80] R. Blumenhagen and E. Plauschinn, Phys. Lett. B **736**, 482 (2014), arXiv:1404.3542 [hep-th].
- [81] F. Marchesano, G. Shiu, and A. M. Uranga, JHEP **09**, 184 (2014), arXiv:1404.3040 [hep-th].
- [82] J. T. Giblin and E. Thrane, Phys. Rev. D **90**, 107502 (2014), arXiv:1410.4779 [gr-qc].
- [83] M. Breitbach, J. Kopp, E. Madge, T. Opferkuch, and P. Schwaller, JCAP **07**, 007 (2019), arXiv:1811.11175 [hep-ph].
- [84] K. Schmitz, JHEP **01**, 097 (2021), arXiv:2002.04615 [hep-ph].
- [85] G. Janssen *et al.*, PoS **AASKA14**, 037 (2015), arXiv:1501.00127 [astro-ph.IM].
- [86] A. Sesana *et al.*, Exper. Astron. **51**, 1333 (2021), arXiv:1908.11391 [astro-ph.IM].
- [87] J. Crowder and N. J. Cornish, Phys. Rev. D **72**, 083005 (2005), arXiv:gr-qc/0506015.
- [88] LISA collaboration, arXiv e-prints, arXiv:1702.00786 (2017), arXiv:1702.00786 [astro-ph.IM].
- [89] T. Robson, N. J. Cornish, and C. Liu, Class. Quant. Grav. **36**, 105011 (2019), arXiv:1803.01944 [astro-ph.HE].
- [90] P. Auclair *et al.* (LISA Cosmology Working Group), Living Rev. Rel. **26**, 5 (2023), arXiv:2204.05434 [astro-ph.CO].
- [91] J. W. Foster, D. Blas, A. Bourgoïn, A. Hees, M. Herrero-Valea, A. C. Jenkins, and X. Xue, (2025), arXiv:2504.15334 [astro-ph.CO].
- [92] R. T. Co, T. Lee, and O. P. Leonard, (2025), arXiv:2508.00979 [hep-ph].
- [93] P. B. Arnold and C.-X. Zhai, Phys. Rev. D **50**, 7603 (1994), arXiv:hep-ph/9408276.
- [94] R. Zambujal Ferreira, A. Notari, O. Pujolàs, and F. Rompineve, Phys. Rev. Lett. **128**, 141101 (2022), arXiv:2107.07542 [hep-ph].